Degradation effects of the active region in UV-C light-emitting diodes

Johannes Glaab,[1,a)] Joscha Haefke,[1] Jan Ruschel,[1] Moritz Brendel,[1] Jens Rass,[1] Tim Kolbe,[1] Arne Knauer,[1] Markus Weyers,[1] Sven Einfeldt,[1] Martin Guttmann,[2] Christian Kuhn,[2] Johannes Enslin,[2] Tim Wernicke,[2] and Michael Kneissl[1,2]

[1]*Ferdinand-Braun-Institut, Leibniz-Institut für Höchstfrequenztechnik, Gustav-Kirchhoff-Str. 4, 12489 Berlin, Germany*

[2]*Technische Universität Berlin, Institut für Festkörperphysik, Hardenbergstr. 36, EW 6-1, 10623 Berlin, Germany*

(Received 7 November 2017; accepted 20 January 2018; published online 12 March 2018)

An extensive analysis of the degradation characteristics of AlGaN-based ultraviolet light-emitting diodes emitting around 265 nm is presented. The optical power of LEDs stressed at a constant dc current of 100 mA (current density = 67 A/cm^2 and heatsink temperature = 20 °C) decreased to about 58% of its initial value after 250 h of operation. The origin of this degradation effect has been studied using capacitance-voltage and photocurrent spectroscopy measurements conducted before and after aging. The overall device capacitance decreased, which indicates a reduction of the net charges within the space-charge region of the pn-junction during operation. In parallel, the photocurrent at excitation energies between 3.8 eV and 4.5 eV and the photocurrent induced by band-to-band absorption in the quantum barriers at 5.25 eV increased during operation. The latter effect can be explained by a reduction of the donor concentration in the active region of the device. This effect could be attributed to the compensation of donors by the activation or diffusion of acceptors, such as magnesium dopants or group-III vacancies, in the pn-junction space-charge region. The results are consistent with the observed reduction in optical power since deep level acceptors can also act as non-radiative recombination centers. *Published by AIP Publishing.*
https://doi.org/10.1063/1.5012608

I. INTRODUCTION

Due to their exceptional properties, such as tailored emission wavelength, low voltage operation, and environmental friendliness, ultraviolet-C (UV-C) light-emitting diodes (LEDs) based on the AlGaN material system are expected to replace conventional mercury gas-discharge lamps in many applications such as water purification,[1] UV curing,[2] and plant growth lighting.[3] However, the lifetime of state-of-the-art deep UV-C LEDs, i.e., LEDs emitting between 200 nm and 280 nm, is still limited to a few 1000 h[4] due to various technological difficulties. First, high densities of threading dislocations[5] and poor ohmic contacts on high Al-content AlGaN[6,7] result in significant Joule heating (increased temperature) in the device during operation, which is known to accelerate degradation.[8,9] Second, the specific epitaxial growth conditions of AlGaN result in a relatively high density of point defects such as hydrogen and carbon impurities, as well as group-III vacancies (V_{Ga}, V_{Al}).[10] These point defects can act as non-radiative recombination centers in the active layers of the device and lower the internal quantum efficiency. Moreover, the point defects can compensate the charge of dopant atoms,[10] thus increasing p- or n-sheet resistivity.[11–13] Various degradation studies on deep-UV LEDs pointed to the generation or propagation of such point defects in or around the active region as the reason for the pronounced reduction of the optical output power.[14–16] In a recent study, Monti *et al.* investigated the degradation behavior of (InAlGa)N-based UV-B LEDs using deep-level transient spectroscopy and photocurrent spectroscopy (PCS).[16] An emerging photocurrent signal during operation at about 2.0–2.5 eV was attributed to the increase in point defects in the electrically active layers which form mid-gap states, act as non-radiative recombination centers, and hence reduce the optical output power. However, none of the degradation studies were able to either precisely locate the degradation areas or identify the defect species.

This paper presents extensive investigations on the constant current and temperature operation induced degradation of AlGaN-based multiple-quantum well (MQW) LEDs emitting at about 265 nm. A combination of voltage-dependent PCS and capacitance-voltage (C-V) measurements allows novel conclusions on the position and nature of point defects, triggering the drop of the optical power during operation.

II. EXPERIMENTAL DETAILS

The UV-C LED heterostructures were grown on epitaxial-lateral overgrown (ELO) AlN/sapphire templates using metalorganic vapor phase epitaxy (MOVPE). Details of the ELO process are described in Ref. 17. The average threading dislocation density (TDD) in the AlGaN layers is about 1×10^9 cm^{-2}. The heterostructure consists of a 1.2 μm thick $Al_{0.8}Ga_{0.2}N$:Si current spreading layer (n-CSL), followed by a 40 nm thick $Al_{0.6}Ga_{0.4}N$:Si buffer layer. The active region consists of three 2-nm-thick $Al_{0.5}Ga_{0.5}N$ quantum wells (QWs), separated by 5-nm-thick partially Si-doped $Al_{0.6}Ga_{0.4}N$ barriers (QBs), followed by a thin

a)Electronic mail: johannes.glaab@fbh-berlin.de

nominally undoped $Al_{0.95}Ga_{0.05}N$ interlayer (IL), an $Al_{0.7}Ga_{0.3}N$:Mg electron-blocking layer (EBL), a 150-nm-thick $Al_{0.32}Ga_{0.68}N/Al_{0.42}Ga_{0.58}N$:Mg short-period superlattice (p-SL), and a thin GaN:Mg cap layer. After MOVPE growth, the wafers were annealed *in-situ* in nitrogen ambient in order to activate the p-dopants. LED chips were fabricated using standard chip-processing technologies. The n- and p-electrodes are based on vanadium (V) and palladium (Pd),[6,18,19] respectively. After dicing the wafers, single chips were flip-chip soldered to aluminum-nitride (AlN) ceramic submounts using gold-tin alloy. The mounted LEDs have a median peak-wavelength of 262 nm, an optical power of about 4.0 mW, and an operation voltage of about 14.5 V at a current of 100 mA.

A batch of five LEDs was attached to a thermoelectric cooler and stressed simultaneously at a constant operation current of 100 mA corresponding to a current density of 67 A/cm^2 in the p-contact and at a constant heatsink temperature of 20 °C in air for 250 h. During operation, the emission spectrum and drive voltage were measured continuously using a spectrometer (AvaSpec ULS2048L UV/VIS) and a switch/multimeter measurement unit (Keithley 2750/E), respectively. Before and after stress, current-voltage (I-V), C-V, and PCS measurements have been conducted. The C-V measurements were performed using an HP 4275A LCR meter operated at a frequency of 1 MHz. The PCS setup is explained in detail in Ref. 20. When operating the LEDs as photodetectors, the excitation light of a defined wavelength was incident from the polished sapphire backside. The photocurrent is induced by absorption in the space-charge regions (SCRs) and was measured at different bias voltages between –2.0 V and 2.0 V using a pico-ampere meter (Keithley 6487). The external quantum efficiency of the photodetector (PCS-EQE) has been calculated from the photocurrent (I_{photo}) using the following formula:

$$PCS-EQE = \frac{I_{photo}}{P_{opt}} \cdot \frac{\hbar \cdot \omega}{q}. \quad (1)$$

Here, P_{opt} is the incident optical power measured using a calibrated reference photodiode, q is the elementary charge, and $\hbar \cdot \omega$ is the photon energy.

III. PRELIMINARY CONSIDERATIONS

For both the interpretation of photocurrent and C-V measurements, some general issues of the SCRs in the LEDs should be stressed first. For this reason, the band diagram of the LED heterostructure, including the different SCRs at the contacts and the pn-junction, as well as the corresponding equivalent circuit of the LED structure, is shown in Figs. 1(a) and 1(b), respectively. The width of the SCR on the n-side (n-SCR) of the pn-junction is larger in comparison to the SCR on the p-side (p-SCR). This can be explained by the higher Mg-doping in the p-side ($\sim 5 \times 10^{19}$ cm^{-3}) compared to the Si-doping in the n-side ($\sim 4 \times 10^{18}$ cm^{-3}). Furthermore, due to its low activation energy of $\leq$25 meV in $Al_{0.6}Ga_{0.4}N$:Si,[21] the Si donors are fully ionized at room-temperature. In contrast, due to the high acceptor ionization energy of Mg in high

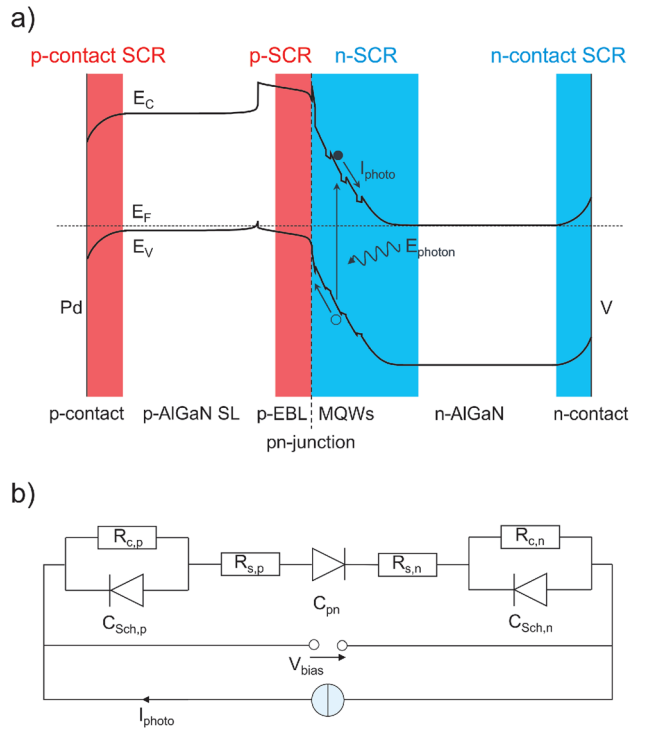

FIG. 1. (a) Schematic of the band diagram of the studied 265 nm UV-C LED with space-charge regions at the metal to semiconductor contacts and the pn-junction. The mechanism of band-to-band photocurrent generation in the pn-junction is illustrated. (b) Simplified equivalent circuit of the corresponding LED structure.

Al-content bulk AlGaN[22] [EBL: E_A ($Al_{0.7}Ga_{0.3}N$) ~400 meV and p-SL: E_A ($Al_{0.4}Ga_{0.6}N$) ~300 meV], only about 1% of the Mg acceptors are ionized at room temperature. However, due to the high electric field at the pn-junction, all acceptors are ionized in the p-side close to the pn-junction as confirmed by band-structure simulations using a one-dimensional drift-diffusion model.[23] As a consequence, the pn-junction can be described as a pn-junction with a wider n-SCR compared to the p-SCR. From simulation data at 0 V, the width of the n-SCR and p-SCR is ~42 nm and ~7 nm, respectively (compare the field distribution simulations presented in Sec. IV).

Furthermore, the p- and n-metal-to-semiconductor contacts are not perfectly ohmic but show a partial Schottky-like behavior, and hence, additional space-charge regions are located at both contacts. These regions are marked as "p-contact SCR" and "n-contact SCR" in Fig. 1(a), and the corresponding reverse-biased Schottky diodes with parallel ohmic behavior are shown in Fig. 1(b). As a consequence, the LEDs exhibit three SCRs connected in series where the width of the pn-SCR decreases, while that of the n- and p-contact SCRs increases with increasing bias voltage (V_{bias}).

IV. RESULTS

Figure 2(a) shows the evolution of the optical power and the forward voltage over time for one representative LED stressed at 100 mA. The inset of Fig. 2(a) shows the emission spectrum at 0 h. A dominant QW emission peak at 262 nm and weak parasitic luminescence between 325 nm and 475 nm can be observed. It should be noted that the peak

wavelength, full width at half maximum (FWHM), or relative intensity of the parasitic peak did not change during operation. For the QW peak, two modes of the reduction of optical power can be identified, as already discussed for (InAlGa)N-based UV-B LEDs in Ref. 8: (1) a fairly rapid reduction of the optical power within the first about 25 h of operation and (2) a slow reduction for operation times >25 h. On average, the optical power dropped by (20 ± 2)% after 25 h and by (42 ± 2)% after 250 h compared to the initial value. The forward voltage decreases within the first hours of operation and increases for longer operation times. The initial reduction of the voltage might be due to heating effects accompanied by a reduction of the sheet resistivity of the AlGaN layers. In contrast, the increase in the voltage indicates an irreversible degradation effect with an increase in the resistivity of the contacts and/or layers.

Figure 2(b) shows characteristic C-V profiles of one LED measured between −1 V and 4 V before and after 250 h of operation. An overall reduction of the capacitance can be observed, which points to reduced space-charges in at least one of the SCRs and a widening of the involved SCRs. Assuming that the operation induced change in the capacitance can fully be ascribed to the pn-junction, the width of the pn-SCR, calculated from the capacitance values at 0 V, is ∼58 nm at 0 h and ∼68 nm at 250 h. How a degradation of the metal-to-semiconductor contacts influences the total capacitance of the LEDs is currently under investigation. Therefore, a final explanation of the operation induced capacitance change cannot be given yet.

Photocurrent spectra have been measured for excitation energies ranging from 3 to 6 eV (about 415 nm to 205 nm) for different bias voltages before and after aging. The PCS-EQE spectra taken at a bias voltage of 0 V before and after operation for 250 h are shown in Fig. 3(a). The PCS-EQE spectrum before aging shows three characteristic steps at 4.6 eV, 5.0 eV, and 5.4 eV marked with (2), (3), and (4) in Fig. 3(a), respectively. The step marked with (2) can be explained by band-to-band absorption and carrier generation in the QWs, whereas the step marked with (3) can be attributed to band-to-band absorption in the quantum barriers (QBs) and, to a minor extent, in the EBL. The classification of steps (2) and (3) is based on calculations of the absorption spectra of the two corresponding layers using fundamental

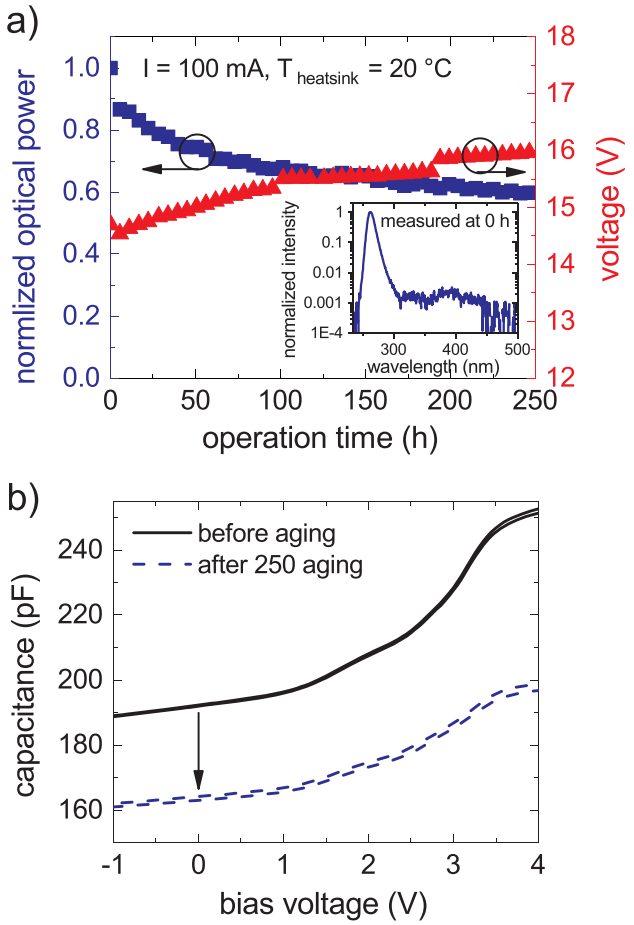

FIG. 2. (a) Integrated optical power (normalized to t = 0 h) and drive voltage as a function of operation time for one representative UV-C LED stressed at 100 mA and 20 °C. The inset shows the emission spectrum of one LED recorded at 100 mA and 0 h. The peak wavelength of the LED is about 262 nm, and a weak parasitic luminescence can be observed around 400 nm. (b) Related C-V characteristics measured as hysteresis between −1 and 4 V before and after 250 h operation at 100 mA and 20 °C. The black arrow emphasizes the decrease in the capacitance during operation.

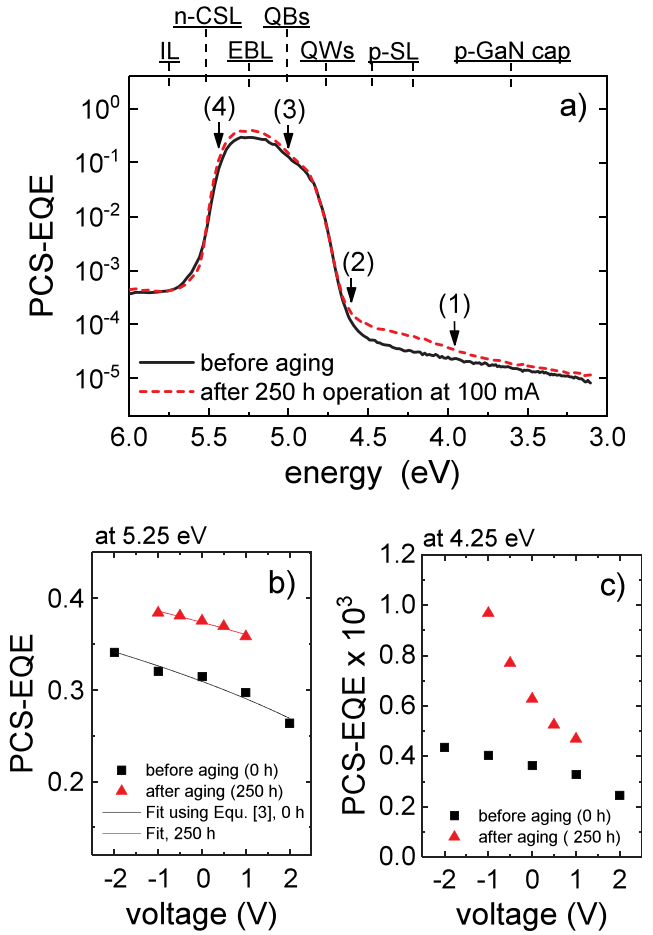

FIG. 3. (a) PCS-EQE extracted from PCS measurements as a function of excitation energy of one representative 265 nm LED biased at 0 V before and after 250 h of operation at 100 mA and 20 °C. Characteristic steps and changes in the spectrum are marked by (1)–(4). (b) and (c) The PCS-EQE at 5.25 eV and 4.25 eV taken from PCS spectra before and after aging, respectively, as a function of bias voltage. The solid lines are fits using Eq. (3). The fit parameters are listed in Table II.

material parameters measured at room temperature in bulk $Al_xGa_{1-x}N$ layers (grown on sapphire substrates by MOVPE), as well as bowing parameters, and the corresponding absorption coefficients presented in Ref. 24. The results of the calculations are shown in Table I and indicate that at 5.25 eV, most of the incident radiation is absorbed in the QBs. Furthermore, the $Al_xGa_{1-x}N$ layers next to the electrodes have higher (n-side: $E_{g,n} \sim 5.6$ eV) and lower (p-side: $E_{g,p} \sim 3.4$ eV to 4.3 eV) bandgap energies compared to the QWs and QBs, which supports the given interpretation of the steps in the PCS-EQE spectrum. The step marked with (4) can be attributed to band-to-band absorption in the $Al_{0.8}Ga_{0.2}N$:Si current spreading layer. This explains the reduction of the PCS-EQE since this layer is isolated from the pn-SCR and therefore no external current signal results.

After aging, two changes in the PCS-EQE spectrum can be observed: First, the maximum value of the PCS-EQE increases, most likely indicating an expansion of the regions in the LED contributing to the photocurrent, e.g., a widening of the pn-SCR further across the 40 nm buffer layer below the lowest QW. Here, it is assumed that the absorption coefficient in the QWs and QBs does not change during aging. Second, a new step appears in the PCS-EQE at about 3.8 eV [marked with (1) in Fig. 3(a)] having a four orders of magnitude lower level compared to the maximum of the PCS-EQE spectrum. This feature might be attributed to increased band-to-band absorption in the p-SL or defect-assisted carrier generation.

Figures 3(b) and 3(c) show the change in the PCS-EQE at 5.25 eV and at 4.25 eV, respectively, as a function of the bias voltage between −2 V and 2 V before and after aging. The PCS-EQE always decreases with increasing bias voltage and increases due to the device operation. The different voltage dependences of the PCS-EQE at 5.25 eV and 4.25 eV indicate different physical origins of the two spectral features, which will be discussed in the following paragraphs.

The reduction of the PCS-EQE with increasing voltage indicates that both spectral features arise from the pn-SCR since only the width of this SCR is reduced with increasing voltage. According to Ref. 25, the relationship between the width of the SCR (W_{SCR}) and the applied voltage (V_{bias}) in a $p^{++}n$-junction is given by

$$W_{SCR} = W_{SCR,p} + W_{SCR,n} \cong W_{SCR,n} = \sqrt{\frac{2\varepsilon_S(V_0 - V_{bias})}{q}\left(\frac{N_A}{N_D(N_A + N_D)}\right)}. \quad (2)$$

Here, $W_{SCR,p/n}$ are the widths of the SCRs in the n- and p-sides of the pn-SCR, ε_s ($= \varepsilon_r \cdot \varepsilon_0$) is the dielectric constant, N_D is the average donor concentration in the n-side, and N_A is the average acceptor concentration in the p-side of the structure. V_0 is the difference of the electrical potential in the valence or conduction band between the n- and p-sides at 0 V and represents the sum of the built-in potential and all changes of the electrical potential due to polarization charge effects within the SCR. Whereas the pn-SCR shrinks with the increasing bias voltage, the SCRs at the p- and n-metal-to-semiconductor contacts expand because both are reverse biased. The dependence of the quantum efficiency (η or PCS-EQE) on W_{SCR} is given by

$$\eta = T[1 - \exp(-\alpha W_{SCR})] = T\left[1 - \exp\left(-\alpha\sqrt{\frac{2\varepsilon_S(V_0 - (F \cdot V_{bias,total})}{q}\left(\frac{N_A}{N_D(N_A + N_D)}\right)}\right)\right], \quad (3)$$

where T is the product of the transmission coefficients at the various interfaces which the light passes, e.g., polished sapphire surface and various heterojunctions in the structure, and α is the absorption coefficient of the layers within the SCR. The left part of Eq. (3) is adapted from Ref. 25 but only takes into account the drift current generated within the SCR, whereas the diffusion current by carriers generated outside and diffused into the SCR is neglected. This assumption is reasonable for two different reasons: On the one hand, the n-layers next to the active region, where most of the absorption happens, have a high Al-content, and therefore, not many carriers are generated outside the pn-SCR for photon energies below 5.5 eV. On the other hand, carriers could be photo-generated in the p-SL for photon-energies below 5.5 eV, but the diffusion of the corresponding electrons (minority carriers in the p-side) towards the n-electrode is hindered by the EBL. The factor F describes the voltage drop across the pn-junction relative to the voltage drop over the entire LED, $V_{bias,total}$, which is the sum of the voltage drops at the contacts, the semiconductor layers, and the pn-junction. This factor could change significantly if the resistivity of the contacts or of certain layers changes during operation.

All results for the PCS-EQE at the 5.25 eV peak point to an increased depletion width on the n-side of the pn-junction due to the degradation. Therefore, Eq. (3) can be used to derive the reduction in the ionized donor concentration affecting the PCS-EQE-bias relation of the pn-SCR. Electrically active donor states, e.g., from Si-dopant atoms

TABLE I. Estimated bandgap energy and absorption of the QWs, QBs, and EBL. Calculations have been conducted using fundamental material parameters of bulk AlGaN layers reported in Ref. 24.

AlGaN layer	Total layer thickness (nm)	Al mole fraction	Bandgap energy (eV)	Absorption at 5.25 eV (%)
QWs	6	0.5	4.68	∼10
QBs	55	0.6	4.97	∼40
EBL	25	0.7	5.26	<1

in the n-side of the pn-SCR, are proposed to be compensated during operation by an increasing number of acceptor states. A detailed discussion on the properties of probable defects inducing such acceptor states can be found in Sec. V. The data shown in Fig. 3(b) were fitted with Eq. (3) using F and N_D as fit parameters, while keeping all other parameters constant. Referring to literature data, α and ε_s were set to $1.2 \times 10^7\,m^{-1}$ and $8 \times 10^{-11}\,Fm^{-1}$, respectively.[24,26] Based on secondary-ion-mass spectrometry (SIMS) measurements of the Mg dopant concentration and assuming full acceptor ionization at the pn-junction, the average acceptor concentration N_A was assumed to be $5 \times 10^{19}\,cm^{-3}$. Furthermore, the built-in voltage V_0 was determined to be 4.84 V by means of self-consistent simulations of the band structure and the carrier concentrations using a one-dimensional drift-diffusion model.[23] The value of V_0 was found to be almost independent of N_D. The transmission T was set to 0.9, which takes into account every reflection at refractive index transitions (e.g., air-to-sapphire and sapphire-to-AlGaN) in the LED. The results of fitting the PCS-EQE at 5.25 eV are shown as solid lines in Figs. 3(b), and the fit parameters are listed in Table II. Accordingly, the donor concentration N_D decreases during 250 h operation from $3.9 \times 10^{18}\,cm^{-3}$ to $2.3 \times 10^{18}\,cm^{-3}$, while F decreases as well. We would like to point out that the reverse case of constant N_D and increasing N_A in the p-side is not likely since even an unrealistically strong increase in N_A in the EBL by two orders of magnitude would still be too small to induce a sufficiently strong widening of the n-SCR. However, the values of N_D before and after aging are realistic since the Si-concentration in the n-side of the LED heterostructures is around $4.0 \times 10^{18}\,cm^{-3}$ as determined by SIMS. The decrease in F most likely corresponds to an increasing resistivity of the contacts and/or layers, but a final explanation cannot be given. When keeping $F = 1$ in the fit, the obtained change in the donor concentration due to aging remains almost the same, but the quality of the fit is reduced.

As already mentioned, the PCS-EQE at 4.25 eV also increases during operation [see Fig. 3(c)]. However, its voltage dependence before aging can probably not solely be attributed to a widening of the pn-SCR as described by Eq. (3) because it is superimposed by the broadening of the PCS-EQE step from the QWs at about 4.6 eV due to the quantum-confined-Stark-effect,[27] which reduces the fundamental band-to-band absorption when an electric field is applied to a polar c-plane QW structure. After aging, the bias dependence of the PCS-EQE at 4.25 eV has changed significantly. Starting from −1 V and increasing the voltage, the decreasing PCS-EQE approaches almost its value before aging. In addition, Eq. (3) cannot be reasonably fitted to the PCS-EQE at 4.25 eV, which motivates two different explanations:

TABLE II. Fitted parameters from fitting Eq. (3) to the PCS-EQE at 5.25 eV as shown in Fig. 3(a).

Parameter	Before aging (0 h)	After aging (250 h)
Donor conc. N_D	$3.9 \times 10^{18}\,cm^{-3}$	$2.3 \times 10^{18}\,cm^{-3}$
Voltage factor F	0.70	0.46

1. Considering the bandgap energies of different layers (see Table I), the photocurrent could be generated in the p-SL and/or the p-GaN cap layer [compare also the marking of the bandgap energies at the top axis in Fig. 3(a)]. Absorption in the p-GaN would fit to the increase in the PCS-EQE at 3.4 eV, whereas absorption in the p-SL would fit to energies between 4.2 eV and 4.4 eV. An increase in the photo-generated electron current from the p-SL across the EBL by trap-assisted tunneling and/or a reduction in the potential barrier during operation could explain the emergence of this spectral feature after 250 h of operation. In addition, the relatively low signal could be explained by the reduced electron transport probability across the potential barrier of the EBL.
2. The spectral feature could be induced by absorption in the pn-junction via acceptor- or donor-like defect states located within the bandgap, e.g., at an energy of about 4.25 eV below the conduction band (acceptor) or above the valence band (donor). The low PCS-EQE signal induced by defect assisted absorption is usually explained by a reduced absorption coefficient due to the low density of states.[28] The broad tail suggests a distribution of defect levels over a large energy range in the bandgap. Assuming that the density of the deep level defects is not constant across the SCR, the voltage dependence of the effective absorption coefficient and, thus, the PCS-EQE-bias dependence can be different from Eq. (3) as it is the case for the PCS-EQE at 4.25 eV after aging.

However, a sound explanation is difficult when keeping in mind that the current under reverse bias and forward bias below the turn-on voltage also increases during aging and its separation from the low photocurrents, as it is observed for voltages ≥ 0 V, becomes difficult. Nevertheless, it should be emphasized that the spectral feature around 4.25 eV after aging is real and not just a measurement artefact induced by the increased current.

To study the proposed increase in the width of the pn-SCR by a reduced donor concentration in the n-side in more detail, self-consistent simulations based on a one-dimensional drift-diffusion model of the LED band structure and the carrier distribution have been performed.[23] Figure 4 shows the calculated electric field in and around the active region for three different donor concentrations ($N_D = 2 \times 10^{18}\,cm^{-3}$, $3 \times 10^{18}\,cm^{-3}$, and $4 \times 10^{18}\,cm^{-3}$) in the n-doped layers. Two effects mainly determine the distribution of the electric field: On the one hand, the electric field is influenced by the space-charge in the pn-SCR, and thus, the electric field steadily decreases with the increasing distance from the pn-junction in both directions. On the other hand, the simulation considers polarization charges at interfaces, e.g., at the QW/QB junctions, which results in abrupt steps of the electric field at the corresponding positions. As expected, the reduction of the average donor concentration leads to an increasing width of the SCR at the n-side ($W_{SCR,n}$ grows), whereas the change at the p-side is negligible ($W_{SCR,p}$ nearly constant). These data fit to the proposed interpretation of the change in the photocurrent feature around 5.25 eV due to aging. At 0 h and 0 V biases, the edge of the n-SCR is located in the first

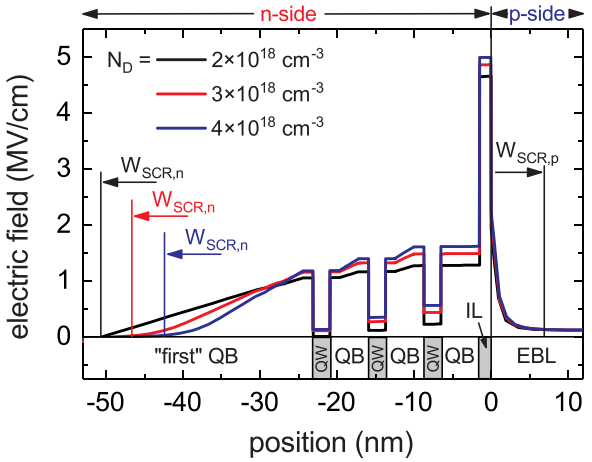

FIG. 4. Calculated electric field distribution around the pn-junction of an UV-C LED structure at 0 V bias for different donor concentrations ($N_D = 2 \times 10^{18}\,cm^{-3}$, $3 \times 10^{18}\,cm^{-3}$, and $4 \times 10^{18}\,cm^{-3}$) in the n-side of the structure. The widths of the SCR in the n-side ($W_{SCR,n}$) are separately marked for different donor concentrations, whereas $W_{SCR,p}$ is almost independent of N_D.

barrier, which corresponds to the blue curve with $N_D = 4 \times 10^{18}\,cm^{-3}$ in Fig. 4. The black curve shows the distribution of the electric field with $N_D = 2 \times 10^{18}\,cm^{-3}$, which roughly corresponds to the proposed situation after 250 h of operation: With increasing operation time, a growing amount of donors is compensated by generated acceptor states in the active region, which leads to a widening of the SCR further into the n-type buffer layer. From the simulated electric field in Fig. 4, the width of the pn-SCR can be determined to be ~50 nm at $N_D = 4 \times 10^{18}\,cm^{-3}$ (0 h) and ~58 nm at $N_D = 2 \times 10^{18}\,cm^{-3}$ (250 h). Thus, the determined change in the width of the pn-SCR is also in good agreement in the C-V characteristic (compare Fig. 2(b), $W_{SCR} \sim 58$ nm at 0 h to ~68 nm at 250 h) and simulation, which supports the consistency of the presented data.

V. DISCUSSION

A comparable reduction of the optical power of AlGaN-based deep UV-C LEDs as shown in Fig. 1(a) has already been reported in the literature. It is commonly explained either by an increase in non-radiative recombination centers in or around the active region of the LEDs or an increase in current paths, shorting the active region.[29,30] Non-radiative recombination usually happens via point defects or extended defects, which form levels deep within the bandgap. The measurement results propose a reduction of the net donor density in the active region which is most likely caused by an increased density of electrically active point defects causing the compensation of the intended doping in the active region and pn-SCR during operation, which is supported by the capacitance reduction, drive voltage increase, and photocurrent increase of the device. In our case, the active region of the LED is n-type (Si-doped QBs and background n-doping in the QWs). Therefore, the observed compensation of donors suggests an increase of acceptors, which fits to the increase of the feature at 5.25 eV in the PCS spectrum and its bias dependence according to Eq. (3). Assuming that the same acceptors are responsible for the increase of the feature at 4.25 eV in the PCS spectrum, the possibly involved defect types can further be narrowed down. The rise of the spectrally broad photocurrent signal at ≥3.8 eV is likely to emerge from an acceptor-like defect band. This would correspond to an energetic position of about (0.9 ± 0.1) eV and (1.2 ± 0.1) eV above the valence band edge in the QWs and the QBs, respectively, which matches the following point defects:

Carbon (C) is a commonly observed impurity in MOVPE-grown III-nitride layers. It can occur in different defect configurations. For example, Wright applied density-functional theory and found that C can act as a compensating acceptor in n-type GaN when substituting nitrogen (C_N).[13] However, from SIMS measurements on UV-C LED structures, we found a C concentration close to the detection limit of $\sim 2 \times 10^{17}\,cm^{-3}$ which is far below the predicted change in the donor concentration.

Magnesium (Mg) is a potential compensating impurity in the n-doped layers of the LED heterostructure worth to consider as it is used as a p-type dopant in the device. Although Mg is not intentionally supplied during growth of the active region, where the activation/generation of point defects during operation is expected, back-diffusion of Mg from the p-side towards the active region during high-temperature growth of the p-side of the heterostructure is a frequently discussed effect.[31] In addition, current and temperature driven diffusion of Mg during device operation, probably assisted by threading dislocations, is a conceivable process. As determined by photoluminescence spectroscopy experiments, Mg forms a deep acceptor level in $Al_xGa_{1-x}N$ (x = 0.27–0.7) at 0.3 eV to 0.4 eV above the valence band edge. This corresponds to an energetic position of about 4.2 eV below the conduction band in $Al_{0.5}Ga_{0.5}N$.[22] Thus, an increase in the Mg content in the active region could explain the observed emergence of the broad tail at ≥3.8 eV in the PCS spectrum.

Group III vacancies, gallium (V_{Ga}) or aluminum vacancies (V_{Al}), and their corresponding defect complexes (V_{III}-X), such as V_{Ga}-$(O_N)^n$ (n = 1, 2, and 3), are also frequently discussed point defects in nitride-based devices. These defects are known to act as compensating acceptors in n-type $Al_xGa_{1-x}N$.[32,33] Due to their low formation energy in n-type and Al-rich $Al_xGa_{1-x}N$, these defects can form in large concentrations during the epitaxial growth of the UV-C LED heterostructures.[34,35] Nam *et al.* investigated transitions between impurity-related charge states in bulk $Al_xGa_{1-x}N$ using photoluminescence[35] and found two broad emission lines, which can be related to donor-acceptor-pair transitions with $(V_{III}\text{-}X)^{2-}$ and $(V_{III})^{3-}$ as deep acceptors and Si or O as shallow donors. For example, the $(V_{III}\text{-}X)^{2-}$ complex forms a deep acceptor level in $Al_xGa_{1-x}N$ with x = 0.50–0.65 (corresponding to the Al-content in the QWs and QBs of the investigated devices) at about 3.0 eV to 3.3 eV below the conduction band edge. This energy also roughly fits to the onset of the aging induced feature in the PCS spectrum at ≥3.8 eV. Furthermore, Dreyer *et al.* reported in a recent study on first-principle calculations with respect to the role of V_{Ga} complexes, more precisely V_{Ga}-3H and V_{Ga}-O_N-2H.[36]

These complexes can act as efficient Shockley-Read-Hall (SRH) recombination centers in InGaN LEDs, i.e., they significantly reduce the internal quantum efficiency of such devices.

All the defects discussed above can act as compensating acceptors in the n-side of UV-C LEDs and hence increase the width of the n-SCR. Furthermore, they can act as centers for non-radiative recombination or parasitic radiative recombination.[22,36] This raises the question how the density of such defects changes during device operation. For example, it is known that especially during the epitaxial growth of Mg-doped AlGaN, high amounts of hydrogen (H) are incorporated,[37] passivating either the Mg acceptor by forming electrically neutral Mg-H defect complexes or group III vacancies by forming the corresponding defect complexes. To break these complexes and to remove the resulting H+ from the layers, a post-growth annealing is introduced. If some Mg-H complexes or isolated H+ remains in the p-doped layers and (unintentionally) also in the active region, these could be broken and propagate during operation due to hot carriers,[38] Joule heating of the device, and re-absorption of UV-radiation. The propagation of Mg dopant atoms into the active region during operation, e.g., by dislocation governed diffusion,[39] could also explain the increase of acceptors in the active region.

Taking into account all observations and their discussion, the following model is proposed for the degradation of the investigated UV-C LEDs: During operation, acceptor-like defects form in or around the active region by activation and/or diffusion, the latter probably assisted by threading dislocations. These defects compensate the n-type doping in and around the active region and act as non-radiative recombination centers. Therefore, the optical output power is reduced, the drive voltage is increased, the capacitance decreases, and the PCS-EQE of the photocurrent rises.

VI. SUMMARY

The degradation effects of AlGaN-based UV-C LEDs emitting at ~262 nm under constant current and temperature operation have been investigated by using PCS and C-V measurements. The optical power of the LEDs reduces rapidly over 250 h of operation to about 58% of its initial value. The reduction of the optical power is accompanied by a reduction of the capacitance and an increase in drive voltage of the device. Furthermore, two changes can be observed in the photocurrent spectrum: First, the photocurrent generated in the QBs, i.e., at 5.25 eV increases, and second, a broad spectral feature emerges between 3.8 eV and 4.5 eV, i.e., energetically below the contributions of QBs and QWs. The increased photocurrent related to the QBs, the reduced capacitance, and the increased drive voltage can be attributed to a reduction of charge states in the n-side of the pn-SCR, most likely by increased defect-induced compensating acceptor states. By analyzing the voltage dependence of the PCS-EQE at 5.25 eV before and after aging, the average change in compensating donor states after aging (which corresponds to the increase in compensating acceptor states) can be estimated to be about $1.6 \times 10^{18}\,\mathrm{cm}^{-3}$. Furthermore, the broad feature in the SPC spectrum at $\geq$3.8 eV is consistent with an increase in compensating acceptors which may be ascribed to Mg impurities or group-III vacancies and related defect complexes. An alternative explanation for this PCS feature would be a photocurrent contribution from the p-SL and/or p-GaN cap layer by electrons tunneling through the EBL. In summary, we propose the following degradation model of the investigated UV-C LEDs: Acceptor-like defects are formed by activation and/or diffusion, the latter probably assisted by threading dislocations. These defects compensate the n-type doping in and around the active region and act as non-radiative recombination centers, hence reducing the optical output power and increasing the drive voltage.

ACKNOWLEDGMENTS

The authors would like to thank the materials technology department and the process technology department at the Ferdinand-Braun-Institut for their contributions in the development of the UV-C LEDs. This work was partially supported by the German Federal Ministry of Education and Research (BMBF) through the consortia project "Advanced UV for Life" under Contract Nos. 03ZZ0106A, 03ZZ0106B, 03ZZ0130A, and 03ZZ0130B. Further support was given by the Federal Ministry for Economic Affairs and Energy (BMWi) through the project "UV-Berlin" under contract 03EFCBE067 and by the Deutsche Forschungsgemeinschaft within the Collaborative Research Center "Semiconductor NanoPhotonics" (CRC 787).

[1]M. A. Würtele, T. Kolbe, M. Lipsz, A. Külberg, M. Weyers, M. Kneissl, and M. Jekel, Water Res. **45**, 1481 (2011).
[2]*III-Nitride Ultraviolet Emitters - Technology and Applications*, edited by M. Kneissl and J. Rass (Springer International Publishing, New York, London/Cham, Heidelberg, 2015).
[3]M. Schreiner, J. Martınez-Abaigar, J. Glaab, and M. Jensen, Opt. Photonik **9**, 34 (2014).
[4]C. Pernot, http://www.nikkiso.co.jp/products/technology/data/technology/technologyE01.pdf for DUV Nitride LEDs: Challenges and Perspectives, Nikkiso CO., LTD; accessed 12 May 2017.
[5]M. Kneissl, T. Kolbe, C. Chua, V. Küller, N. Lobo, J. Stellmach, A. Knauer, H. Rodriguez, S. Einfeldt, Z. Yang, N. M. Johnson, and M. Weyers, Semicond. Sci. Technol. **26**, 014036 (2011).
[6]M. Lapeyrade, S. Alame, J. Glaab, A. Mogalitenko, R.-S. Unger, Ch. Kuhn, T. Wernicke, P. Vogt, A. Knauer, U. Zeimer, S. Einfeldt, M. Weyers, and M. Kneissl, J. Appl. Phys. **122**, 125701 (2017).
[7]X. A. Cao, H. Piao, S. F. LeBoeuf, J. Li, J. Y. Lin, and H. X. Jiang, Appl. Phys. Lett. **89**, 082109 (2006).
[8]J. Glaab, Ch. Ploch, R. Kelz, Ch. Stölmacker, M. Lapeyrade, N. Lobo Ploch, J. Rass, T. Kolbe, S. Einfeldt, F. Mehnke, Ch. Kuhn, T. Wernicke, M. Weyers, and M. Kneissl, J. Appl. Phys. **118**, 094504 (2015).
[9]Z. Gong, M. Gaevski, V. Adivarahan, W. Sun, M. Shatalov, and M. Asif Khan, Appl. Phys. Lett. **88**, 121106 (2006).
[10]C. G. Van de Walle and J. Neugebauer, J. Appl. Phys. **95**, 3851 (2004).
[11]A. P. Polyakov and I.-H. Lee, Mat. Sci. Technol. R **94**, 1 (2015).
[12]S. Nakamura, N. Iwasa, M. Senoh, and T. Mukai, Jpn. J. Appl. Phys., Part 1 **31**, 1258 (1992).
[13]A. F. Wright, J. Appl. Phys. **92**, 2575 (2002).
[14]M. Meneghini, D. Barbisan, L. Rodighiero, G. Meneghesso, and E. Zanoni, Appl. Phys. Lett. **97**, 143506 (2010).
[15]C. G. Moe, M. L. Reed, G. A. Garrett, A. V. Sampath, T. Alexander, H. Shen, M. Wrabeck, Y. Bilenko, M. Shatalov, J. Yang, W. Sun, J. Deng, and R. Gaska, Appl. Phys. Lett. **96**, 213512 (2010).
[16]D. Monti, M. Meneghini, C. De Santi, G. Meneghesso, E. Zanoni, J. Glaab, J. Rass, S. Einfeldt, F. Mehnke, J. Enslin, T. Wernicke, and M. Kneissl, IEEE Trans. Electron Devices **64**, 1 (2016).

[17]V. Kueller, A. Knauer, C. Reich, A. Mogilatenko, M. Weyers, J. Stellmach, T. Wernicke, M. Kneissl, Z. Yang, L. C. Chua, and N. M. Johnson, IEEE Photonics Technol. Lett. **24**, 1603 (2012).
[18]J. Rass, T. Kolbe, N. Lobo Ploch, T. Wernicke, F. Mehnke, Ch. Kuhn, J. Enslin, M. Guttmann, Ch. Reich, A. Mogilatenko, J. Glaab, Ch. Stölmacker, M. Lapeyrade, S. Einfeldt, M. Weyers, and M. Kneissl, Proc. SPIE **9363**, 93631K (2015).
[19]M. Lapeyrade, A. Muhin, S. Einfeldt, U. Zeimer, A. Mogilatenko, M. Weyers, and M. Kneissl, Semicond. Sci. Technol. **28**, 125015 (2013).
[20]M. Brendel, A. Knigge, F. Brunner, S. Einfeldt, A. Knauer, V. Kueller, U. Zeimer, and M. Weyers, J. Electon. Mater. **43**, 833 (2014).
[21]Y. Taniyasu, M. Kasu, and N. Kobayashi, Appl. Phys. Lett. **81**, 1255 (2002).
[22]M. L. Nakarmi, N. Nepal, J. Y. Lin, and H. X. Jiang, Appl. Phys. Lett. **94**, 091903 (2009).
[23]*Simulations are Based on the Software Package SiLENSe 5*.2.1 (STR Group, Ltd.).
[24]M. Röppischer, "Optische eigenschaften von aluminium-galliumnitrid-halbleitern," Ph.D. dissertation (Südwestdeutscher Verlag für Hochschulschriften, Saarbrücken, 2011).
[25]S. M. Sze and K. K. Ng, *Physics of Semiconductor Devices*, 3rd ed. (John Wiley & Sons, Inc., New Jersey, 2007).
[26]V. W. L. Chin, T. L. Tansley, and T. Osotchan, J. Appl. Phys. **75**, 7365 (1994).
[27]D. A. B. Miller, D. S. Chemla, T. C. Damen, A. C. Gossard, W. Wiegmann, T. H. Wood, and C. A. Burrus, Phys. Rev. Lett. **53**, 2173 (1984).
[28]V. Lebedev, I. Cimalla, U. Kaiser, and O. Ambacher, Phys. Status Solidi C **1**(2), 233 (2004).
[29]M. Meneghini, D. Barbisan, Y. Bilenko, M. Shatalov, J. Yang, R. Gaska, G. Meneghesso, and E. Zanoni, Microelectron. Reliab. **50**, 1538 (2010).
[30]A. Pinos, S. Marcinkevicius, J. Yang, R. Gaska, M. Shatalov, and M. S. Shur, J. Appl. Phys. **108**, 093113 (2010).
[31]K. Köhler, T. Stephan, A. Perona, J. Wiegert, M. Maier, M. Kunzer, and J. Wagner, J. Appl. Phys. **97**, 104914 (2005).
[32]C. G. Van de Walle, C. Stampfl, and J. Neugebauer, J. Cryst. Growth **189**/**190**, 505 (1998).
[33]C. Stampfl and C. G. Van de Walle, Phys. Rev. B **65**, 155212 (2002).
[34]T. Mattila and R. M. Nieminen, Phys. Rev. B **55**, 9571 (1997).
[35]K. B. Nam, M. L. Nakarmi, J. Y. Lin, and H. X. Jiang, Appl. Phys. Lett. **86**, 222108 (2005).
[36]C. E. Dreyer, A. Alkauskas, J. L. Lyons, J. S. Speck, and C. G. Van de Walle, Appl. Phys. Lett. **108**, 141101 (2016).
[37]S. Nakamura, T. Mukai, M. Senoh, and N. Iwasa, Jpn. J. Appl. Phys., Part 1 **31**, 139 (1992).
[38]S. M. Myers and A. F. Wright, J. Appl. Phys. **90**, 5612 (2001).
[39]S. Tomiya, T. Hino, S. Goto, M. Takeya, and M. Ikeda, IEEE J. Quantum Electron. **10**, 1277 (2004).